Noncanonical Interactions in the Management of RNA Structural Blocks by the Transcription Termination Rho Helicase†

Annie Schwartz,‡ Céline Walmacq,§,|| A. Rachid Rahmouni,‡ and Marc Boudvillain*,‡

Centre de Biophysique Moléculaire (UPR4301), CNRS, rue Charles Sadron, 45071 Orléans cedex 2, France, and Ecole doctorale Sciences et Technologies, Université d'Orléans, Orléans, France

Received March 12, 2007; Revised Manuscript Received May 10, 2007

ABSTRACT: To trigger transcription termination, the ring-shaped RNA−DNA helicase Rho from *Escherichia coli* chases the RNA polymerase along the nascent transcript, starting from a single-stranded C-rich *Rut* (Rho utilization) loading site. In some instances, a small hairpin structure divides harmlessly the C-rich loading region into two smaller *Rut* subsites, best exemplified by the tR1 terminator from phage λ. Here, we show that the Rho helicase can also elude a RNA structural block located far downstream from the single-stranded C-rich region but upstream from a reporter RNA−DNA hybrid. In this process, Rho hexamers do not melt the intervening RNA motif but require single-stranded RNA segments on both of its sides. The reaction is also favored by physiological glutamate ions and can implicate Rho primary recognition of 5′-YC dimers (as for *Rut* binding) significantly upstream (>70 nucleotides) from the intervening motif. Surprisingly, we also found that primary interactions of Rho with 2′-hydroxyl groups located upstream from the intervening RNA structure serve to elude the motif. This demonstrates that the preference of Rho for RNA residues is not limited to the secondary interaction site that mediates ATPase-fuelled mechanochemistry within the hexamer central channel. These features could be part of an energy-effective mechanism in which Brownian exploration of the conformation of the Rho−substrate complex and accommodation of downstream secondary structures within a composite primary interaction site replace ATP-dependent translocation of the Rho enzyme along corresponding structured portions of the RNA chain.

Transcription termination factor Rho from *Escherichia coli* is a ring-shaped hexameric helicase that loads onto ∼70-nucleotide (nt),[1] C-rich, and usually scarcely structured segments of the nascent transcript called *Rut* (for Rho utilization) sites (*1*, *2*). This interaction in turn triggers ATP-dependent translocation of the Rho hexamer toward the growing transcript 3′-end where Rho eventually dissociates the transcription complex (*1*, *2*). The initial formation of a productive Rho−transcript complex is an elaborate process that is only partially understood. Each Rho monomer contains a primary interaction subsite that captures specifically a 5′-YC dimer through a steric "key−lock" fit of the pyrimidine rings and specific contacts with the Watson−Crick edge of the 3′-C residue (*3*, *4*). Importantly, this interaction does not implicate the 2′-hydroxyl groups of the 5′-YC dimers (*3*, *4*) which is consistent with Rho primary binding to model C-rich RNA and DNA strands occurring with similar affinities (*5*−*7*). Moreover, the hexamer configuration requires zigzagging stretches (≥12 nt) of a single-stranded nucleic acid (NA) to span the distance between adjacent primary subsites (*8*). These NA stretches are disordered in the crystal structures of Rho−NA complexes (*4*, *8*, *9*), yet they can be engaged in additional sequence-specific contacts with the enzyme (*10*), though the molecular details of this interaction remain unknown. Moreover, the inward crownlike disposition of the primary interaction subsites along the hexamer as well as the marked helical twist of the open Rho ring (*8*), a likely intermediate species (*11*), is thought to drive the transcript 3′-end into the central Rho channel. There, RNA-specific contacts with the Rho secondary binding site likely mediate Rho's ATPase-driven mechanochemistry (*9*). The most probable state of a translocating Rho motor is thus a closed hexamer that encircles its RNA substrate within a constricted central channel (*9*). Taken together, these features suggest that Rho should not easily accommodate structured portions of the nascent transcript, yet experimental data indicate otherwise. For instance, RNA secondary structures embedded within the λtR1 *Rut* site (e.g., cognate boxB hairpin or artificial MS2F5 aptamer) turn on rather than impair Rho action (*12*−*14*). RNA structures located downstream from a *Rut* site can also have unexpected effects on the Rho enzyme. In one intriguing study, RNA helices (in the form of oligoribonucleotides annealed to the transcript) could block Rho translocation and unwinding of downstream RNA−DNA hybrids, whereas a cognate RNA hairpin could not (*15*). This suggested that Rho could specifically ignore certain RNA structures, possibly by bridging the base of their helical stem (*15*). The "looping out" of RNA structures has

† This research was funded in part by the Agence Nationale de la Recherche (PCV06-135253), the Ligue contre le Cancer (Région Centre), the Association pour la Recherche sur le Cancer (#3639), and Biotechnocentre.

* To whom correspondence should be addressed. Phone: +33 238 25 55 85. Fax: +33 238 63 15 17. E-mail: boudvill@cnrs-orleans.fr.

‡ CNRS.

§ Université d'Orléans.

|| Present address: National Cancer Institute, National Institutes of Health, Frederick, MD 21702-1201.

[1] Abbreviations: NA, nucleic acid; nt, nucleotide; *Rut*, Rho utilization; TEC, transcription elongation complex.

10.1021/bi700493m CCC: $37.00
Published on Web 07/27/2007

also been proposed to explain the downstream shift of the termination window that occurs when the secondary structure content is increased within the nascent transcript (*16*, *17*). A mechanism involving helicase stepping across steric roadblocks could represent a rational alternative to purposeless NA or protein dissociation events. Existing data suggest several molecular pathways that may authorize such a mechanism. Structural roadblocks may be looped out in transient open states of the hexamer ring during translocation (*18*), and/or the hexamer central channel may have sufficient conformational plasticity [as observed for the SV40 helicase (*19*)] to selectively engulf given native RNA structures. Alternatively, Rho may productively accommodate RNA structures into an outer binding site, as suggested by electron micrographs of tRNA bound to Rho (*20*).

To assess how Rho deals with structural blocks, we have performed helicase experiments with multipiece NA substrates. We show that the hexameric helicase can indeed "ignore" secondary structures such as forked RNA junctions intercalated between a synthetic loading site [*aRut* site (*21*)] and a reporter RNA−DNA helix. Moreover, the data suggest a mechanism whereby composite primary transcript binding is used by Rho to elude intervening structural blocks in a way that is reminiscent of the interaction with the otherwise compact and C-rich λtR1 terminator. However, the putative RNA binding site appears to be rather flexible as it can extend significantly from the ~50 nt, C-rich *aRut* region to include a distant (>70 nt) downstream secondary structure. Under in vitro saturating helicase conditions, the RNA binding site can also be reduced to a minimal forked motif that is poor in properly spaced and single-stranded 5′-YC dimers. In this case, however, unforeseen primary interactions between Rho and the 2′-OH groups of nucleotides located in the upstream arm of the forked motif become mandatory. These data reveal that noncanonical interactions with structural components of the transcript can also participate in the formation of a competent complex with Rho. Thus, one economical means devised by the Rho enzyme for overcoming RNA structure obstacles could be to accommodate them in alternative entry sites. This suggests that the Rho motor can operate from multiple starting points and could contribute to an explanation for why Rho-dependent termination clusters are often dispersed over a large template region as each Rho entry site should give rise to a distinct set of transcript release sites.

MATERIALS AND METHODS

Materials. Chemicals, enzymes, and oligonucleotides were purchased from Sigma-Aldrich, New England Biolabs, and Biomers.net, respectively. The Rho protein (concentrations expressed in hexamers throughout the paper) and long (>400 nt) poly[rC] fragments were obtained as described previously (*18*).

Oligonucleotides encoding the R^3 sequences were subcloned between the *Hpa*I and *Acc*65I (or *Sma*I) sites of the pSP73 plasmid (Promega) to yield plasmids pCW06 (R^{3c} sequence) and pCW07 (R^{3u} sequence). The R^5 sequence is encoded by plasmid pAS02 (*22*). The DNA fragments encoding the R^{5del1} and R^{5del2} sequences downstream from a T7 promoter were obtained by PCR amplification of the pAS02 plasmid with appropriate primers.

Preparation of the Substrates. The transcripts were obtained by in vitro transcription of the DNA templates with T7 RNA polymerase, as described previously (*23*). The R^5 chimeras were obtained by splinted ligation of appropriate RNA and DNA strands with T4 DNA ligase (*24*).

For most substrates, 10 pmol of the ^{32}P-labeled NA strand was mixed with 1.1 molar equiv of the unlabeled NA strands in 20 μL of hybridization buffer [150 mM AcK, 20 mM HEPES (pH 7.5), and 0.1 mM EDTA] and heated for 2 min at 95 °C. The mixtures were slowly cooled to room temperature before being mixed with 5 μL of native buffer (15% Ficoll-400 and 0.1 M EDTA). The multipiece substrates were then purified from the reaction mixture by 7% native PAGE and stored at −20 °C in standard helicase buffer [20 mM HEPES (pH 7.5), 0.1 mM EDTA, 0.5 mM DTT, and 150 mM AcK].

Helicase Assays. In a typical helicase reaction, 0.15 pmol of NA substrate was mixed with 0.6 pmol of Rho hexamers in 27 μL of helicase buffer and incubated for 3 min at 30 °C. Then, 3 μL of a solution containing ATP and $MgCl_2$ (1 mM, final concentrations) and NA traps (oligonucleotides complementary to the O^n sequence and the 3′-end of R^5, respectively; 12 pmol, each) in helicase buffer were added to the mixture before further incubation at 30 °C. Reaction aliquots were taken at various times and mixed with 4 volumes of quench buffer (100 mM EDTA, 2.5% SDS, and 15% Ficoll-400) before being loaded on 7.5% polyacrylamide gels that contained 1× TBE and 0.5% SDS. Detection and quantification of gel bands were performed with a Storm-860 Phosphorimager and related software (Molecular Dynamics).

For single-run helicase experiments, poly[rC] in excess (3 μM in rC residues) was added to the initiation mix (*18*). For most time courses, individual kinetic parameters were obtained by fitting data points to the equation $F_p = A(1 - e^{-kt}) + k't$, where F_p is the fraction of product formed, A is the amplitude of the exponential phase of the reaction, and k and k' are the rate constants of the exponential and linear phases of the reaction, respectively. Note that for reactions exhibiting pseudo-first-order kinetics, k' was set to zero. Kinetic parameters for the evolution of intermediate species were derived from the equation $F_t = F_{max}k_1/(k_s - k_1)(e^{-k_1t} - e^{-k_st})$, where F_t and F_{max} are the transient and maximal fractions of intermediate species, respectively, while k_1 and k_s are the rate constants for the formation and decay of the intermediate species, respectively.

RESULTS

Design of Multipiece RNA−DNA Substrates. Rho unwinds RNA−DNA hybrids located downstream from a *Rut* site more efficiently than RNA helices (*15*, *25*). At a low Mg^{2+} concentration (0.4 mM), a RNA oligonucleotide hybridized to a *Rut*-containing transcript blocked Rho translocation, thereby preventing unwinding of a downstream RNA−DNA helix (*15*). In contrast, an intervening RNA stem−loop structure did not alter Rho's RNA−DNA helicase activity, but it was unclear if the hairpin motif was melted in the process (*15*). We used these and other previous observations to design multipiece RNA−DNA substrates giving rise to distinct reaction products depending on how Rho deals with intervening RNA secondary structures (Figure 1A). The

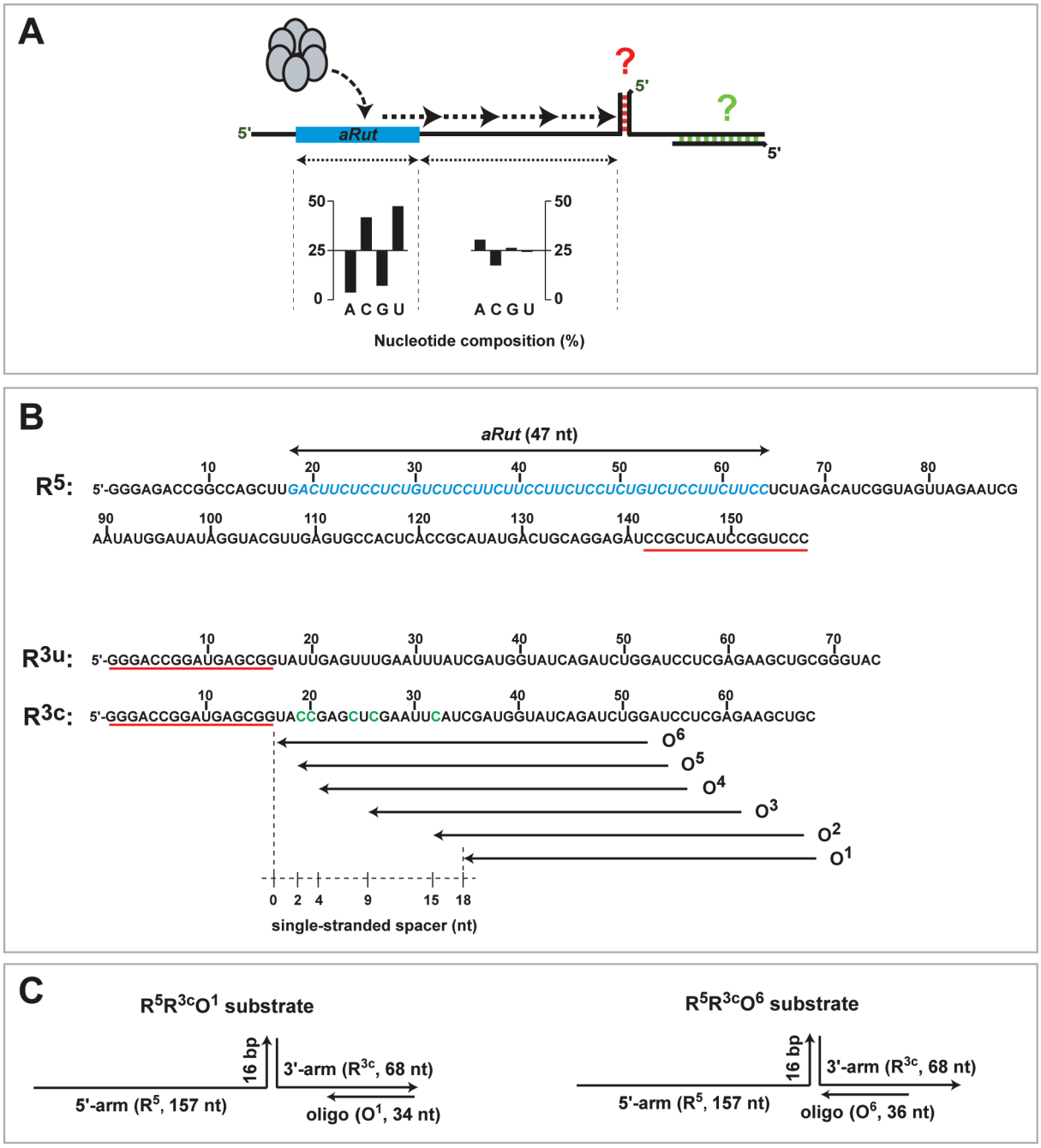

FIGURE 1: Multipiece constructs used in the helicase experiments. (A) Experimental rationale. The constructs are made of two distinct RNA arms which form a forked junction upon pairing of complementary sequences (red dashes). An artificial Rho loading site [*aRut* site, colored blue (*18*, *21*)] and a reporter RNA−DNA helix (green dashes) are located on opposite sides of the RNA junction (red dashes). Products of a helicase reaction should depend on how Rho copes with the intervening junction (red and green question marks). Base composition (in percent) is provided below the diagram for major single-stranded RNA regions. (B) RNA components of the multipiece constructs. The complementary sequences yielding the forked junction are underlined in red. The nucleotides that are different in the R^{3c} and R^{3u} arms are colored green. The hybridization positions of the various reporter oligonucleotides (O^1−O^6) are indicated by arrows. (C) Schematic of two representative multipiece constructs.

substrates were made of two distinct RNA halves, R^5 and R^3 [R^{3u} or R^{3c} (Figure 1B)] and contained a single synthetic Rho loading site [*aRut* site (*18*, *21*)] in the upstream section of R^5. Pairing of R^5 and R^3 creates a RNA forklike junction downstream from the *aRut* site, as an intervening RNA hairpin would (Figure 1A). The *aRut* site was separated from the forked junction by an ~80 nt random sequence (Figure 1A,B) to prompt the assembly of a functional Rho motor upstream from the junction. The constructs also contained a "reporter" oligodesoxyribonucleotide (O^n) annealed to various sections of the ^{32}P-labeled R^3 arm (Figure 1B,C). Nearest-neighbor calculations (*26*, *27*) indicated that the corresponding RNA−DNA hybrids are significantly more stable ($\Delta G_{hyb} < -45$ kcal/mol) than the R^5R^3 junction ($\Delta G_{hyb} = -34.9$ kcal/mol). Thus, factors other than helix stability would have to account for any selective unwinding of the reporter RNA−DNA hybrids.

Because of the design of the substrates, we envisioned three outcomes for Rho action. If the forked RNA junction blocks or induces dissociation of the Rho hexamers, the substrates should not be altered during the course of a helicase experiment ($R^5R^3O^n$ product). In contrast, melting

of the junction upon translocation of Rho from the *aRut* site should separate the two substrate's arms but prevent Rho-catalyzed release of the reporter oligonucleotide (R^5 and R^3O^n products). Finally, if the Rho helicase can step over RNA structures, the RNA junction should remain intact while the downstream RNA−DNA hybrid is unwound (R^5R^3 and O^n products).

Rho Can Elude a RNA Structural Block. Helicase experiments were first performed under multiple-turnover conditions (with respect to the NA substrate) with the $R^5R^{3u}O^1$ construct and an excess of Rho hexamers in standard helicase buffer [150 mM AcK, 20 mM HEPES (pH 7.5), 0.1 mM DTT, and 0.1 mM EDTA (*18*, *22*)] at 30 °C. Rho−substrate complexes were allowed to form before initiation of the helicase reaction with a mix of ATP, $MgCl_2$, and trap oligonucleotides (to prevent reannealing of any substrate's NA strand released during the reaction). Then, reaction aliquots were removed at various times, mixed with SDS quench buffer, and analyzed by nondenaturing PAGE (see Materials and Methods).

During the initial phase of the helicase reaction (<5 min), Rho converts most of the $R^5R^{3u}O^1$ construct (80%) into a bipartite RNA product (R^5R^{3u}) from which the reporter oligonucleotide (O^1) had been stripped (Figure 2A). In contrast, disruption of the RNA junction within $R^5R^{3u}O^1$ (yielding R^5 and $R^{3u}O^1$) is a less frequent event (19%), although it occurs at a comparable rate (Figure 2A). This distribution of primary reaction products was confirmed in experiments in which the ^{32}P label was on the O^1 oligonucleotide rather than on the R^{3u} strand (Figure 2B, gel and left graph). At longer incubation times, however, the major R^5R^{3u} product is further unwound into R^5 and R^{3u} components, an event that can be detected only when the R^{3u} strand is labeled (Figure 2A). This secondary reaction may also correspond to a branched pathway with a strong bias toward eluding the RNA junction. This could contribute to the slow apparent rate of the reaction ($<0.05\ min^{-1}$) since most helicase runs would leave the R^5R^{3u} intermediate intact (futile helicase turnovers). On the other hand, the fraction of the minor primary product ($R^{3u}O^1$) remains stable at long incubation times (Figure 2A,B) which indicates that Rho cannot form a productive complex with this RNA−DNA species. These results were hardly affected by the duration of preincubation (0−60 min), the order of addition of Rho, $R^5R^{3u}O^1$, and Mg^{2+}/ATP cofactors, or the use of a substrate bearing a slightly different downstream arm ($R^5R^{3c}O^1$ construct; Figure 2C and data not shown). Helicase experiments were also performed with $R^5R^{3u}O^1$ in the presence of an excess of poly[rC] in the initiation mix to trap the Rho molecules that are unbound as well as the ones that are released during the first enzyme turnover [single-run conditions (*18*, *28*)]. Under these conditions, ∼40% of the $R^5R^{3u}O^1$ construct was unwound by Rho (Figure 2B, right graph), a percentage that falls in the normal range for single-run unwinding of *aRut*-containing substrates of comparable stability (*22*). Moreover, the addition of the poly[rC] trap did not modify the kinetic regimen (pseudo-first order; in Figure 2B, compare graphs) or the rates of formation ($k_1 \sim 0.8\ min^{-1}$ and $k_2 \sim 0.4\ min^{-1}$ at 30 °C) or distribution ($A_1/A_2 \sim 4$) of reaction products. This indicates that enzyme cycling (to form new competent Rho−substrate complexes under multirun conditions) is not rate-limiting with $R^5R^{3u}O^1$ and that the frequency of helicase runs is similar for the two competing reaction pathways (RP1 and RP2 in Figure 2A). This also shows that Rho-directed unwinding of the R^3O^1 helix downstream from the intervening RNA structure (RP1) is the dominant reaction outcome irrespective of the kinetic conditions (single vs multiple turnovers; Figure 2B). Thus, the Rho helicase can leave untouched a RNA secondary structure (in the form of a forked junction) located far downstream from a *Rut* site yet remove roadblocks (such as the O^1 oligonucleotide) located at even further downstream transcript positions.

Unwinding of the Reporter Helix Does Not Occur if the Downstream Arm of the Substrate Is a DNA Strand (D^{3u}). To comprehend better the mechanism used by Rho to elude the forked junction, several variants of the composite substrate were probed. First, the downstream RNA arm was replaced with a cognate DNA strand ($R^5D^{3u}O^1$ construct). Helicase experiments were performed with $R^5D^{3u}O^1$ under the standard multirun conditions described above. Rho did not remove the reporter oligonucleotide from $R^5D^{3u}O^1$ (RP1), but it unwound the intervening RNA−DNA junction [R^5 and $D^{3u}O^1$ products (Figure 2D)]. This reaction exhibited classical biphasic (pre-steady-state) kinetics (*18*, *28*), which contrasts with the experiments performed with the $R^5R^3O^1$ substrates (Figure 2A−C) and indicates that Rho cycling is slower on $R^5D^{3u}O^1$ [$k_{linear\ phase} < 0.02\ min^{-1}$ at 30 °C (Figure 2D)]. Moreover, only ∼20% of $D^{3u}O^1$ was released during the first helicase turnover [$k_{exponential\ phase} \sim 0.4\ min^{-1}$ (Figure 2D)]. This suggests that Rho-directed unwinding of the intervening NA junction (RP2 in Figure 2A) is always a low-frequency event and that it is not strongly influenced by the nature of the released strand. On the other hand, Rho action beyond the junction (RP1) absolutely required RNA residues in the downstream arm of the substrate (compare panels A and D of Figure 2). This implies that unwinding of the reporter helix, when it occurs, is directly related to Rho's RNA-dependent ATPase (*5*) [and thus helicase (*29*)] activity and does not stem from indirect events occurring at or upstream from the junction. Rho may thus behave similarly with the forked RNA and RNA−DNA junctions while not being able to proceed further along a downstream DNA arm.

Eluding the Forked RNA Junction Requires Adjacent Single-Stranded Segments. Helicase experiments were also performed with composite substrates in which the location of the reporter RNA−DNA helix was varied systematically between two extreme positions along the R^3 arm (Figure 1B,C). These constructs contained a few U → C mutations in the downstream arm [R^{3C} arm (Figure 1B)] because the original R^{3u} arm did not yield sufficiently stable RNA−DNA derivatives [$R^5R^{3u}O^1$ excepted (data not shown)]. As shown in Figure 3A, the position of the reporter hybrid (with respect to the forked RNA junction) influenced dramatically the reaction outcome. With $R^5R^{3c}O^6$ (where the hybrid and junction helices are contiguous), RP2 became the only reaction pathway (Figure 3A, left panel). Complete inhibition of RP1 (R^5R^{3c} product) did not result from the juxtaposition of the two helices since it was also observed with the $R^5R^{3c}O^3$ construct (Figure 3A, middle panel). In fact, a significant distance between the junction and reporter helices was required for RP1 to occur (>9 nt) or become predominant [>15 nt (Figure 3A, right panel and graph)]. Thus, preservation of the RNA junction helix during a Rho helicase run

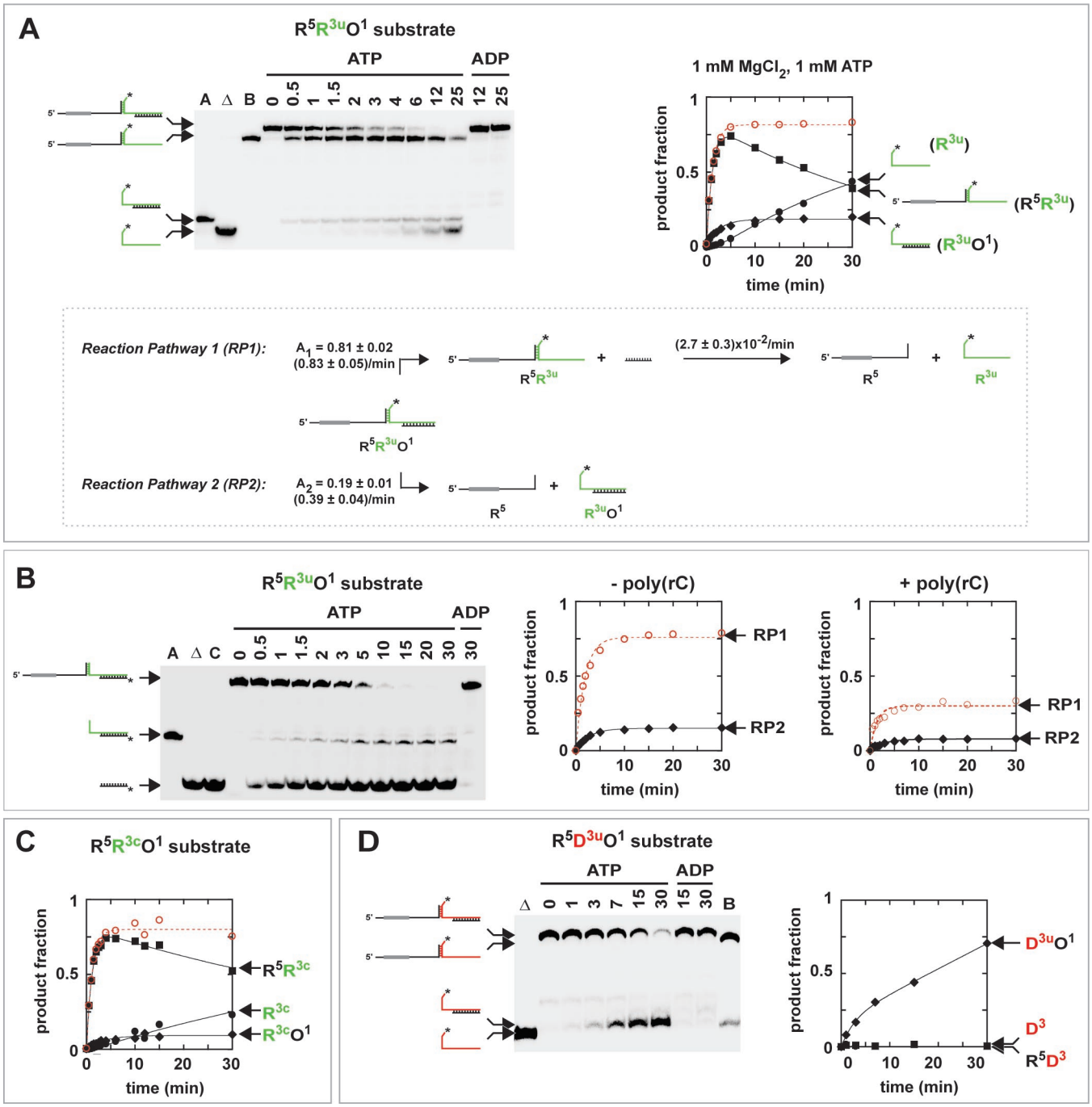

FIGURE 2: Rho-directed unwinding of the multipiece constructs. Helicase experiments were performed with three-piece constructs in which the downstream arm was either a RNA (A−C) or DNA (D) strand (the positions of the ^{32}P labels are indicated with asterisks). The constructs (5 nM) were incubated for 3 min at 30 °C with an excess of Rho hexamers (20 nM) in standard helicase buffer (*18*). The helicase reactions were initiated by the addition of $MgCl_2$ (1 mM), ATP (1 mM), and trap oligonucleotides (400 nM each). In single-run assays, an excess of poly[rC] was also included in the initiation mixture (*18*, *28*). In control experiments, ATP was replaced by ADP. At various times (indicated in minutes above the gel lanes), aliquots were removed from the helicase mixtures and analyzed by 7.5% PAGE in the presence of 0.5% SDS [to denature Rho−NA complexes (*18*)]. Control R^3O^1 and R^5R^3 (or R^5D^3) constructs were also assembled separately and loaded on the gels (lanes A and B). The ^{32}P end-labeled O^1 oligonucleotide was loaded in lane C. Lanes marked with Δ correspond to heat-denatured reaction aliquots. The graphs show the fractions of ^{32}P-labeled products released from the multipiece constructs as a function of time (black filled squares and circles correspond to data for RP1 primary and secondary products, respectively; data for total RP1 products are depicted by open red circles; diamonds represent data for RP2 products). The curves are Kaleidagraph (Synergy Software) fits of the data to equations describing the kinetic scheme shown in panel A. Equations describing a two-step reaction (R^5R^3 intermediate and R^3 final products) and pseudo-first-order progress of total RP1 products (dashed red curves) were used to determine RP1 amplitude and rates. The progress of the D^3O^1 product (panel C) was best described by a pre-steady-state mechanism (*18*, *28*).

requires a minimal single-stranded RNA segment downstream from the junction.

To determine whether a similar rule applies for the other side of the RNA junction, we prepared a multipiece substrate ($R^5O^{R8}R^{3u}O^1$) containing an additional RNA−DNA helix (R^5O^{R8}, 24 bp) ending 4 nt upstream from the R^5R^3 junction. With this construct, Rho-induced dissociation of the RNA junction (RP2; $R^{3u}O^1$ product) was predominant (Figure 3B);

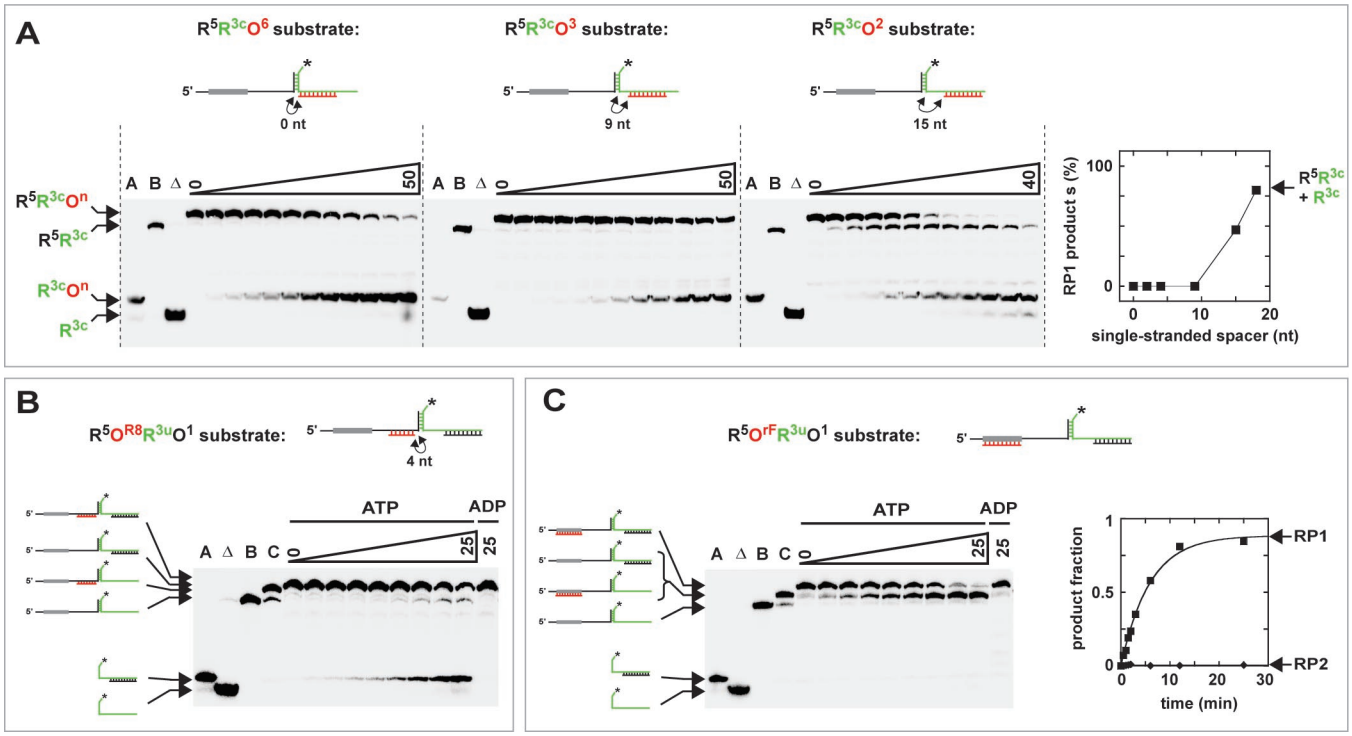

FIGURE 3: Effect of RNA−DNA hybrids on Rho-dependent disruption of multipiece substrates. Helicase experiments were performed as described in the legend of Figure 2 with the constructs displayed in each panel. Reaction time frames (in minutes) are also depicted above each gel. The R^3O^n, R^5R^3, and $R^5R^3O^1$ constructs were loaded in control lanes A−C, respectively. Filled squares and diamonds correspond to total RP1 and RP2 products, respectively. (A) Representative gels and graph showing the dependence of helicase products on the distance between the RNA junction and reporter hybrid. (B) A RNA−DNA helix located upstream from the RNA forked junction inhibits unwinding of the reporter hybrid. (C) Shielding of the *aRut* site with the O^{rF} oligonucleotide selectively abolishes RP2. Substrate assembly and helicase assays were performed in sodium acetate to prevent multiplex structures with the purine-rich O^{rF} oligonucleotide (*18*). Under these conditions, pseudo-first-order parameters for formation of RP1 products were as follows: $A_1 = 0.88 \pm 0.02$ and $k_1 = 0.17 \pm 0.01$ min^{-1}.

R^5R^{3u} and R^{3u} species constituted a small fraction of reaction products [~15% (Figure 3B)] likely arising from an impaired RP1 (with, possibly, transient formation of $R^5O^{R8}R^{3u}$ or $R^5R^{3u}O^1$). These data reveal that a double-stranded region (R^5O^{R8} helix) upstream from the RNA junction is also sufficient for critically altering the reaction outcome. It follows that Rho eluding the forked RNA junction is a context-dependent event that requires single-stranded RNA regions on both sides of the junction (see also below).

Productive Rho Binding Despite Shielding of the aRut Site. The data presented above indicate that intervening RNA motifs can remain in a native conformation while Rho proceeds toward downstream transcript regions. We wanted to ensure that during this process Rho loads initially at the expected position (*aRut* site), significantly upstream (>70 nt) from the RNA junction. Toward this end, we prepared the $R^5O^{rF}R^{3u}O^1$ construct in which the O^{rF} oligonucleotide is paired to the *aRut* sequence. We expected this NA helix to prevent productive interaction of Rho with $R^5O^{rF}R^{3u}O^1$. Indeed, sequestering of *aRut* residues into Watson−Crick base pairs inhibited Rho-dependent termination of transcription (*21*) or helicase action (*18*) with other NA substrates. With $R^5O^{rF}R^{3u}O^1$, however, shielding of the *aRut* site did not completely inhibit Rho function. While RP2 products were no longer detected, unwinding of the reporter RNA−DNA helix still occurred to a full extent, albeit at a slower rate [$k_1 = 0.17$ min^{-1} (Figure 3C)]. This result suggests that RP1 and RP2 stem from distinct Rho binding modes. In one case, the anticipated association of Rho (*1*, *2*) with the high-affinity (C-rich) upstream single-stranded sequence (*aRut*) initiates enzyme tracking along the R^5 strand and unwinding of the intervening RNA junction (RP2). In the other case, singular and alternative interaction of Rho with the substrate (i.e., implicating double-stranded C-rich and/or single-stranded C-poor regions; see also Figures 1A and 1B) leaves the forked RNA junction intact but still promotes a functional Rho conformation able to dissociate the downstream reporter helix (RP1).

Effects of Experimental Conditions on the Competing Reaction Pathways. Although mechanistically informative, alternative reaction pathways may lack biological significance if they require conditions that are too peculiar or permissive. To assess the generality of our results, we have performed helicase experiments with the prototypical $R^5R^{3u}O^1$ construct under a variety of experimental conditions. First, we varied the helicase concentration which affected the rate of $R^5R^{3u}O^1$ decay at the lowest Rho concentrations (Figure 4A, left panel). This result is consistent with a switch from a pseudo-first-order to a pre-steady-state kinetic regimen (with slower enzyme cycling) under subsaturating Rho conditions (*28*) and with the respective maximal fractions of $R^5R^{3u}O^1$ that can be converted during the first helicase run. In contrast, the distribution of reaction products hardly changed with the Rho:substrate ratio [$A_1/A_2 \sim 4$ (Figure 4A, right, and data not shown)] which indicates that the distribution of reaction products observed initially (Figure 2A) was not due to a differential saturation of competing binding sites.

We also examined the RP1 and RP2 responses to modifications of the salt composition of the helicase mixture. We first tested the two Mg^{2+}/ATP conditions that either

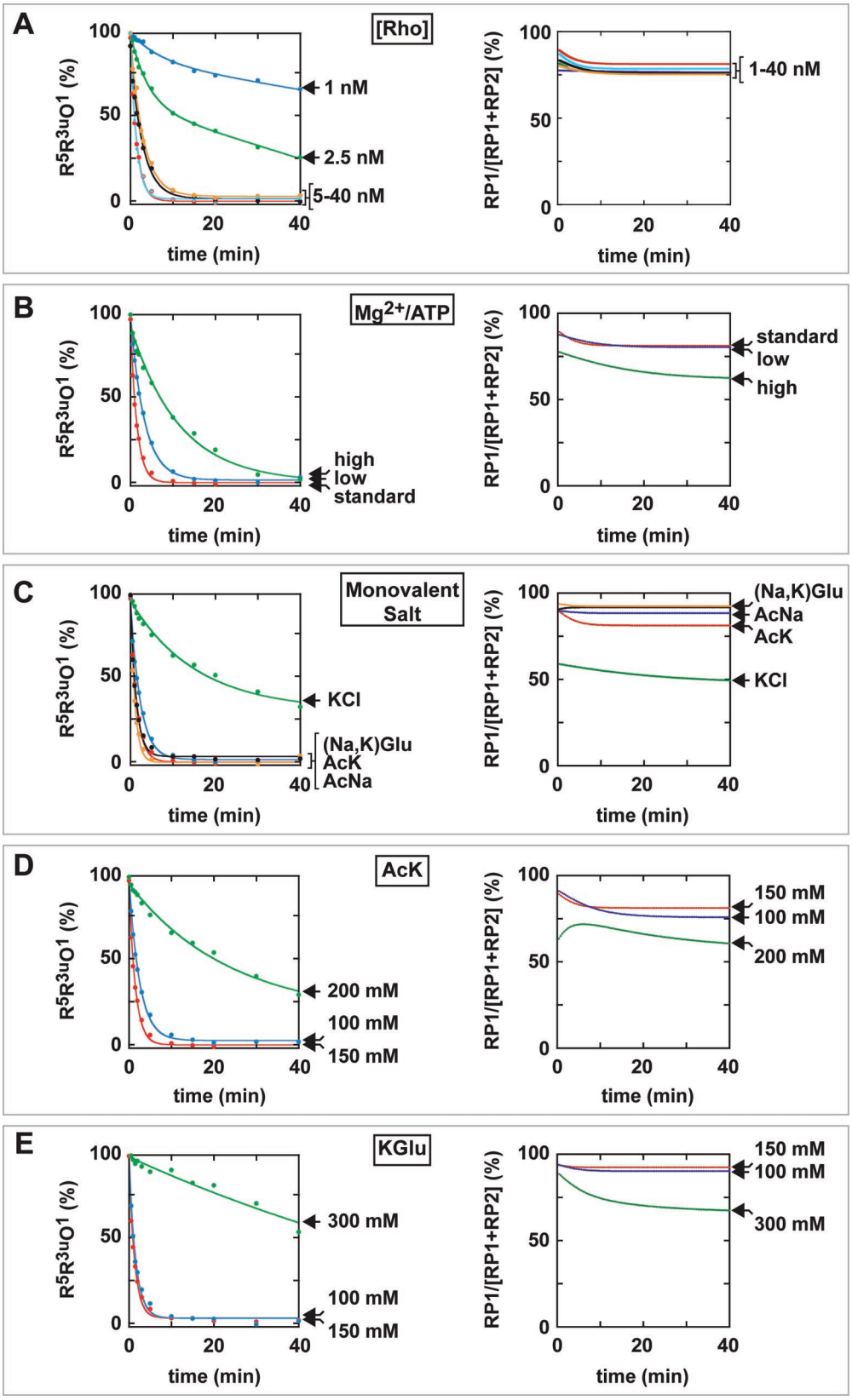

FIGURE 4: Influence of reaction conditions on the two competing helicase pathways. In the left panels, the curves are fits to equations describing pseudo-first-order (saturating Rho concentrations) or pre-steady-state (subsaturating Rho concentrations) decay of the $R^5R^{3u}O^1$ substrate. The curves in the right panels are Kaleidagraph simulations of the evolution of the product ratios as a function of time. They were obtained from interspersed RP1 and RP2 product fractions that were automatically generated by Kaleidagraph from actual kinetic fits (such as the ones shown in Figure 2). With the exception of the individual parameter analyzed in each panel, helicase reactions were performed under standard conditions. (A) Effect of the Rho concentration (from 1 to 40 nM). The concentration of $R^5R^{3u}O^1$ was kept constant (5 nM). (B) Effect of the concentrations of Mg^{2+} and ATP cofactors. Reactions were initiated with 0.4 mM Mg^{2+} and 2 mM ATP (low), 1 mM Mg^{2+} and 1 mM ATP (standard), or 4 mM Mg^{2+} and 5 mM ATP (high). (C) Effect of the nature of monovalent salts (150 mM each). (D and E) Effect of the concentrations of monovalent salts.

inhibited ("low" conditions, 0.4 mM Mg^{2+} and 2 mM ATP) or allowed ("high" conditions, 4 mM Mg^{2+} and 5 mM ATP) Rho-dependent dissociation of an RNA strand from the *trpt′* transcript (*15*, *25*). As shown in Figure 4B (left panel), the two sets of conditions slowed $R^5R^{3u}O^1$ decay when compared to our standard conditions (1 mM Mg^{2+} and 1 mM ATP). However, only the high conditions, which have the largest kinetic effect (Figure 4B, left panel), also affected the distribution of reaction products (right panel). The larger fraction of RP2 products formed under these conditions is consistent with the facilitation of RNA unwinding at high Mg^{2+} and ATP concentrations (*15*, *25*), yet RP1 products still accounted for more than half of the total reaction products under these conditions (Figure 4B). Moreover, the non-negligible amounts (~20%) of RP2 products formed under the low and standard conditions (Figure 4B) show that Rho disruption of RNA helices is not always fully controlled by adjustment of Mg^{2+} and ATP concentrations.

Changes in the monovalent salts present in the helicase mixture also altered the branched reaction pathway with $R^5R^{3u}O^1$ (Figure 4C). Notably, RP1 was favored by the presence of sodium or glutamate ions and, in any case, gave rise to ≥50% of the reaction products. Conversely, RP2 products were usually formed in smaller proportions which, however, increased in the presence of potassium and chloride ions (Figure 4C). Increasing the ionic strength of the reaction mixture also slightly favored RP2 over RP1 (Figure 4D,E) but, at the same time, slowed significantly $R^5R^{3u}O^1$ decay (Figure 4D,E). When conditions known to favor RP2 were combined (150 mM KCl with 4 mM $MgCl_2$ and 5 mM ATP), Rho-directed unwinding of $R^5R^{3u}O^1$ was 4−5 times slower than under standard conditions, yet RP1 still accounted for ~35% of the reaction output (data not shown). Thus, RP1 is not a trivial alternative to canonical Rho action from the high-affinity *aRut* site (*18*, *21*) but rather constitutes a robust and likely ubiquitous component of the reaction framework.

Productive Interaction of Rho with Minimal Forked Substrates. To better define substrate features important for the alternative RP1, we prepared another series of composite substrates containing modified R^5 arms. First, we tested the $R^{5del1}R^{3u}O^1$ construct which lacks the first 80 nt of the R^5 arm [including the *aRut* sequence (Figure 5A)]. Under standard helicase conditions (20 nM Rho, 150 mM AcK, 1 mM Mg^{2+}, and 1 mM ATP), Rho did not react with $R^{5del1}R^{3u}O^1$ (Figure 5B, left gel). When the nature of the monovalent salt present in solution was changed, however, RP1 could be selectively restored with this construct (Figure 5B, right gel and graph). As for the "full-length" $R^5R^{3u}O^1$ substrate (Figure 4C) but in a more dramatic way, glutamate ions were the best RP1 activators. This strong salt dependence was distinctive of the minimal forked substrates and was not observed with more "classical" *aRut*-containing substrates [Figure 5C and data not shown (*18*)]. On the other hand, pairing of the O^{R8} oligonucleotide to the upstream arm of $R^{5del1}R^{3u}O^1$ suppressed Rho-directed unwinding of this construct (Figure 5A and data not shown). This indicates that, as for the longer $R^5R^{3u}O^1$ substrate ($R^5O^{R8}R^{3u}O^1$ construct in Figure 3B), a single-stranded region upstream from the forked junction is required for RP1 to occur.

One noticeable feature of $R^{5del1}R^{3u}O^1$ is its limited potential for canonical sequence-specific interactions (*3*, *4*, *10*, *30*). For instance, given the positions of 5′-YC dimers within $R^{5del1}R^{3u}O^1$ (Figure 5A) and the ~35 Å spacing of primary (YC-bearing) binding clefts along the Rho hexamer (*8*), no more than two monomer subsites can be filled by the same substrate molecule. This number can even be reduced to one, as in the $R^{5del2}R^{3u}O^1$ substrate (Figure 5A), provided that the Rho concentration is increased [Figure 5D and data not shown; note that 100 nM remains well below the physiological concentration of Rho which is in the micromolar range (*31*)]. These data suggest that the reactivity of $R^{5del1}R^{3u}O^1$ and $R^{5del2}R^{3u}O^1$ (Figure 5D) rests largely on substrate components distinct from canonical sequence-specific Rho interacting partners. Additional helicase experiments revealed that the double-stranded RNA junction itself is important. Indeed, deletion of the junction motif, to yield the "linear" $R^{5-3\Delta junction}O^1$ substrate, severely impairs unwinding of the reporter RNA−DNA helix (Figure 6A). The presence of RNA residues within the R^{5del1} arm is even more critical, as evidenced by the complete loss of Rho helicase activity upon replacement of R^{5del1} with a cognate DNA strand (data not shown). To locate the important 2′-hydroxyl moieties more precisely, we prepared minimal forked substrates with R^{5del1} chimeras wherein either the 5′-single-stranded portion of R^{5del1} ($[^{5'}DR]^{5del1}R^{3u}O^1$ substrate) or the region involved in pairing with R^3 ($[^{5'}RD]^{5del1}R^{3u}O^1$ substrate) was made of DNA residues. Although Rho did not react with $[^{5'}DR]^{5del1}R^{3u}O^1$, it unwound $[^{5'}RD]^{5del1}R^{3u}O^1$ as efficiently as the parental $R^{5del1}R^{3u}O^1$ substrate (Figure 6B). Thus, a number of 2′-hydroxyl groups that are critical to Rho-directed unwinding of the downstream $R^{3u}O^1$ helix (RP1) in fact stand within the single-stranded NA region that is located on the other (upstream) side of the forked junction.

5′-YC Dimers Upstream from the Forked Junction Can Boost RP1. Although the minimal forked substrates (Figure 5A) are unwound by Rho in an ATP-dependent fashion [$k_1 \sim 0.04$ min^{-1} in KGlu (Figure 5B)], they are not as reactive as *aRut*-containing or *λ*tR1-derived RNA−DNA substrates [$0.1 < k_{obs} < 1$ min^{-1} at 30 °C (Figures 2 and 4; A. Schwartz, A. R. Rahmouni, and M. Boudvillain, manuscript in preparation; *18*, *22*)]. We also mentioned earlier that shielding of the *aRut* site of $R^5R^{3u}O^1$ by a complementary oligonucleotide slows RP1 (Figure 3C). These observations suggest that elements of the canonical Rho primary interaction with pyrimidine residues (*4*, *10*) also stimulate RP1. To test this proposal, we ligated a DNA oligonucleotide containing the *aRut* sequence (D^{aRut}) to the upstream end of $R^{5del1}R^{3u}O^1$. Rho unwinding efficiency was improved significantly with this chimeric substrate, in terms of both the reaction rate ($k_1 \sim 0.25$ min^{-1}) and the weaker dependence on monovalent salts (Figure 6C), which supports the proposal. Moreover, RP2 products were re-observed with this construct [$A_2 \sim 0.1$ and $k_2 \sim 0.25$ min^{-1} in AcK (Figure 6C)] which confirms that RP2 relies on canonical, RNA-independent, Rho primary contacts to the *aRut* sequence. Yet, for RP2, R^5 ribose moieties located downstream from the *aRut* site are necessary, most likely to be engaged in the Rho secondary site interactions that mediate the enzyme's mechanochemistry (*5*, *9*, *32*, *33*). This is evidenced by the absence of RP2 products with $[D^{aRut}D^{5del1}]R^{3u}O^1$, a substrate containing an "all-DNA" upstream half (Figure 6D). In sharp contrast, Rho triggers formation of RP1 products from the $[D^{aRut}D^{5del1}]$-$R^{3u}O^1$ substrate (Figure 6D). This reaction occurs at a rate that is moderate (0.05 min^{-1} at 30 °C) but comparable to

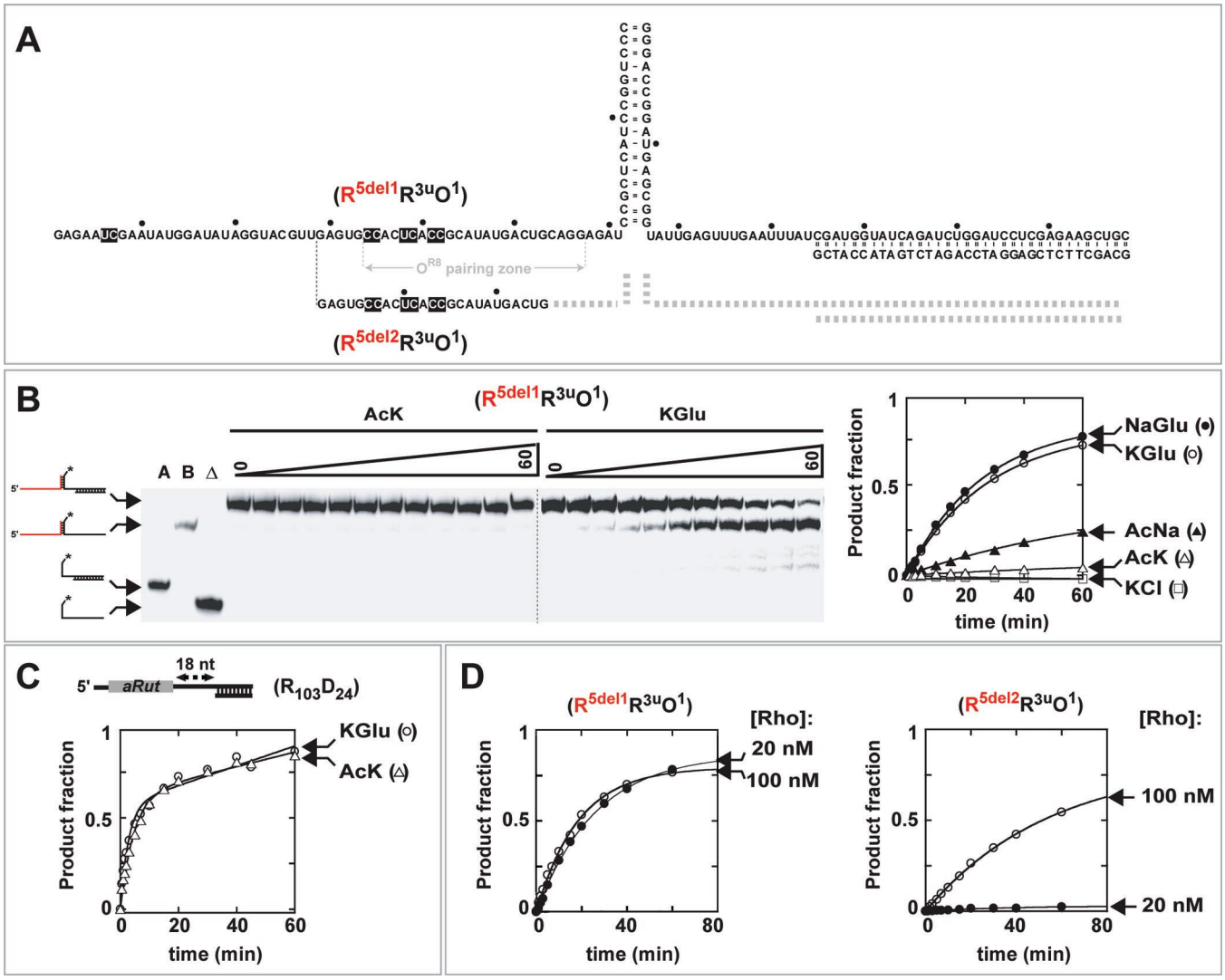

FIGURE 5: Rho-directed unwinding of minimal forked RNA−DNA substrates. Reactions were performed under standard conditions unless stated otherwise. (A) Schematic of the substrates with an increasing number of deletions (encompassing the *aRut* motif) at the 5′-end of the R^5 arm. Single-stranded 5′-YC dimers are identified by black boxes. (B) Effect of monovalent salts on Rho-directed unwinding of $R^{5del1}R^{3u}O^1$. Lanes A and B correspond to control $R^{3u}O^1$ and $R^{5del1}R^{3u}$ constructs, respectively. Lane Δ refers to a heat-denatured reaction aliquot. Reaction time frames (in minutes) are shown above the gel. (C) Unwinding of the linear $R_{103}D_{24}$ substrate (*22*) is not affected by the nature of the monovalent salt. (D) Effect of the length of the upstream arm on Rho activity. Reactions were performed in the presence of 150 mM KGlu. Note that only RP1 products could arise from the minimal forked substrates.

that of RP1 decay of the $R^{5del1}R^{3u}O^1$ and $[^5'RD]^{5del1}R^{3u}O^1$ substrates [0.04 min^{-1} (Figure 6B)]. Overall, helicase experiments indicate that full RP1 activation [k_1 > 0.2 min^{-1} at 30 °C (Figures 2A,C and 6C)] is achieved through additive Rho interactions with distinct substrate components (2′-hydroxyl moieties and pyrimidine residues) located upstream from the forked junction (compare panels B−D of Figure 6). Moreover, the absence of a single-stranded C-rich stretch (Rut site) can be compensated partially with glutamate ions (Figure 5B) which, however, cannot offset the lack of 2′-hydroxyl groups upstream from the forked junction (Figure 6D). Finally, we note that the reactivity of the $[D^{aRut}D^{5del1}]$-$R^{3u}O^1$ substrate (Figure 6D) implies that, for RP1, the ribose-specific contacts that are thought to mediate ATP-dependent Rho physical work within the hexamer central channel (*5*, *9*, *32*, *33*) do not implicate the upstream arm of the substrate. The data thus also demonstrate that Rho can form at least two distinct types of productive tertiary interactions with the 2′-OH groups of RNA substrates.

A Complex Set of Productive RP1 Interactions. Equilibrium binding measurements indicate that Rho binds to $R^{5del1}R^{3u}O^1$ only ~3 times less tightly than to the parental $R^5R^{3u}O^1$ substrate (Table 1). An effect similar in magnitude was observed upon shielding the *aRut* site of linear RNA−DNA substrates with a complementary oligonucleotide [which inhibited substrate unwinding in this case (*18*)]. Moreover, the affinities of Rho for the $R^5R^{3u}O^1$ and $[D^{aRut}D^{5del1}]R^{3u}O^1$ substrates are very similar (Table 1). These data show that contacts between Rho and *aRut* residues do not contribute more than 10% of the total ground-state binding energy and that the respective contribution of interactions of Rho with 2′-OH moieties of the upstream substrate's arm is negligible. They thus also confirm that equilibrium binding parameters are usually poor predictors of the reactivity of helicase substrates (*18*, *34*−*36*). This is probably because, in most cases, activation of the complexes involves the formation of enzyme−substrate tertiary contacts that are distinct from ground-state interactions. This explana-

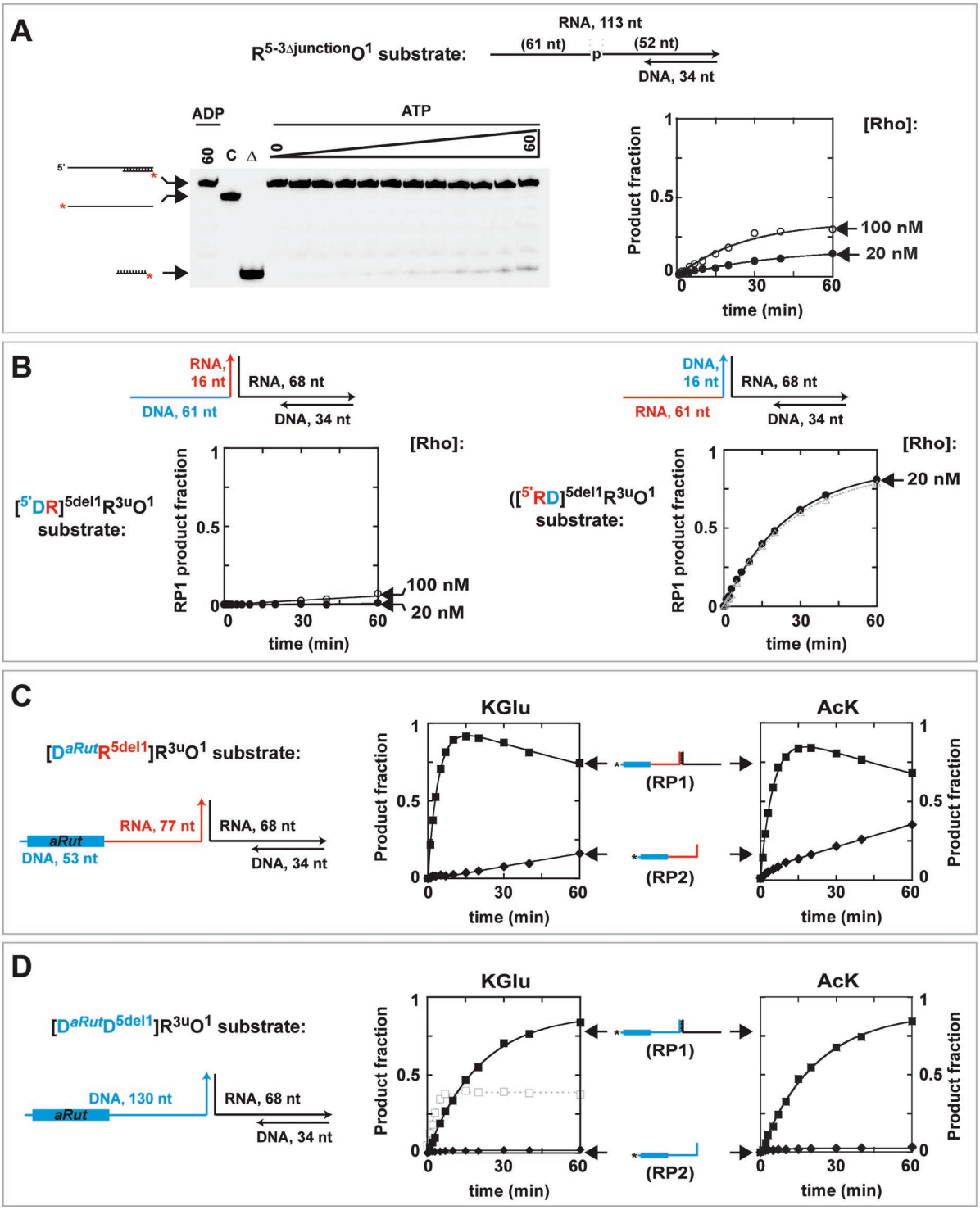

FIGURE 6: Specific features of the minimal forked RNA−DNA substrates are important for Rho helicase efficiency. Helicase reactions were performed in the presence of 1 mM ATP, 1 mM $MgCl_2$, and 150 mM KGlu unless stated otherwise. (A) Deletion of the intervening double-stranded RNA junction severely impairs Rho helicase activity. The DNA template for transcription of $R^{5-3\Delta junction}$ was obtained by PCR amplification of synthetic oligonucleotides. The gel shows a representative helicase reaction performed over a 60 min period with $R^{5-3}\Delta^{\Delta junction}O^1$ (5 nM substrate, 20 nM Rho hexamers). In control lane C, the $R^{5-3}\Delta^{\Delta junction}$ transcript bears the ^{32}P label (depicted with an asterisk), whereas in other gel lanes, the ^{32}P label is on the O^1 oligonucleotide. Lane Δ refers to a heat-denatured reaction aliquot. (B) DNA residues upstream from the junction helix inhibit RP1. The composition of the substrate chimeras is depicted schematically above the graphs. The kinetic profile of the reaction with $R^{5del1}R^{3u}O^1$ (empty gray triangles and dashed curve) is also shown for comparison. (C) An *aRut*-containing DNA oligonucleotide ligated upstream from the R^{5del1} arm stimulates RP1 and reactivates RP2. For technical reasons, The ^{32}P label is on the upstream arm. (D) RP1 does not require RNA residues in the substrate's upstream arm provided that an *aRut* sequence is present. A control substrate with a scrambled sequence instead of the *aRut* sequence was inactive (not shown). The empty gray squares and dotted curve correspond to the formation of RP1 products in the presence of 3 μM poly[rC] (single-run conditions).

tion seems particularly relevant for Rho−RNA complexes which undergo various rearrangements on the "activation" pathway, some of which are ATP-dependent (*8*, *9*, *11*).

To evaluate Rho−substrate interactions under a more functional context, we have also performed helicase experiments with the $R^{5del1}R^{3u}O^1$ and $[D^{aRut}D^{5del1}]R^{3u}O^1$ substrates

Table 1: Equilibrium Binding Parameters for Interaction of Rho with Representative Forked Substrates[a]

substrate	*aRut* site	F_{max}	n	K_d (nM)	ΔG (kcal/mol)
$R^5R^{3u}O^1$	yes	0.50 ± 0.08	1.38 ± 0.16	0.67 ± 0.13	−12.8
$R^{5del1}R^{3u}O^1$	no	0.55 ± 0.10	0.82 ± 0.17	2.18 ± 0.40	−12.1
$[D^{aRut}D^{5del1}]R^{3u}O^1$	yes[b]	0.56 ± 0.03	1.59 ± 0.24	0.72 ± 0.07	−12.8

[a] Samples were equilibrated for 10 min at 30 °C in 20 mM HEPES (pH 7.5), 0.1 mM EDTA, 0.5 mM DTT, and 150 mM KGlu before analysis with a filter binding assay, as described previously (*18*). F_{max} is the maximal fraction of ^{32}P-labeled substrate retained on the nitrocellulose membrane; K_d is the dissociation constant, and n is the Hill coefficient (*18*). Parameters were averaged from at least two independent experiments. [b] The upstream arm of the substrate, including the *aRut* region, is made of DNA residues.

in the presence of poly[rC] or poly[dC] competitor (single-round conditions; see Materials and Methods). Under these conditions, unwinding of the minimal $R^{5del1}R^{3u}O^1$ substrate was competitively inhibited by the presence of either poly[C] molecule in the initiation mix (data not shown). This inhibition contrasts with the efficient single-run unwinding of the parental $R^5R^{3u}O^1$ substrate (Figure 2B). However, it is not necessarily surprising given that with $R^{5del1}R^{3u}O^1$ at least four empty primary subsites per Rho hexamer are available for direct interaction with a high-affinity poly[C] molecule (see above). Once bound to the Rho−substrate complex, the poly[C] strand may thus easily invade (and displace $R^{5del1}R^{3u}O^1$ from) the remaining primary subsites and/or central channel [these processes are expected to be fast with poly[rC] (*11*)], thereby preventing $R^{5del1}R^{3u}O^1$ unwinding. Thus, the minimal forked RNA substrates would likely require additional cis-acting components for RP1 to occur in competitive environments. In contrast, poly[C] fragments did not inhibit RP1 with the suboptimal but C-rich $[D^{aRut}D^{5del1}]R^{3u}O^1$ substrate. Indeed, ~40% of $[D^{aRut}D^{5del1}]$-$R^{3u}O^1$ was unwound in the presence of poly[rC] (Figure 6D, gray open squares and dotted curve). Surprisingly, however, the helicase reaction was significantly faster ($k_1 \sim 0.37$ min^{-1}) than under multirun conditions, an acceleration that was also observed in the presence of poly[dC] (data not shown). Although idiosyncratic poly[C] effects are not unprecedented (*18*), they urge caution in interpreting single-run experiments with the Rho helicase. Yet, together with the other helicase and equilibrium binding data, these results attest that maximization of a Rho−substrate assembly competent for RP1 is a complex multistep process involving various types (and/or sets) of tertiary interactions, some of which can implicate additional NA cofactors.

DISCUSSION

Most of the RNA helicases that have been studied in vitro require a single-stranded NA segment to load productively onto their substrate (*37*, *38*). In the complex cell environment, however, RNA transcripts are often highly structured molecules, coated with proteins, which fold as they emerge from the ternary transcription complex (*39*, *40*). Thus, unless the helicases load directly on the emerging transcript [as RNA processing factors recruited by the C-terminal domain of RNA polymerase II might do (*39*)], they may have to deal with structural impediments to their initial interaction with the RNA chain. In the case of the Rho helicase, an alternative solution has evolved in the form of biased C-rich/G-poor transcript sequences which yield unstructured *Rut* motifs caught by the enzyme (*1*, *2*). Once bound to the transcript, Rho can disrupt downstream roadblocks such as hybridized NA strands or the ternary transcription complex. It has been suggested, however, that Rho dissociation activity may not be totally indiscriminate, especially when particular RNA motifs are considered (*15*, *25*). To evaluate this possibility, we have performed helicase experiments with composite NA substrates containing a single-stranded *aRut* loading site and an intervening RNA forked junction upstream from a reporter RNA−DNA helix (Figure 1). Unexpectedly, we have found that Rho hexamers can unwind the reporter hybrid without melting the intervening RNA structure. This behavior is part of a branched reaction pathway in which selective unwinding of the reporter hybrid (RP1) occurs for a much larger fraction of substrate molecules than does melting of the forked junction [RP2 (Figure 2A−C)].

What is the underlying molecular mechanism for the general preference of RP1 over RP2 (Figures 2A−C and 4 and data not shown)? Data presented herein strongly suggest that the minor reaction pathway (RP2) corresponds to the expected mode of action of Rho, i.e., primary Rho anchoring to a C-rich single-stranded *Rut* site followed by ATPase-driven 5′ → 3′ translocation along the RNA chain and disruption of downstream roadblocks (*1*, *2*). For instance, RP2 is inhibited by pairing of a complementary oligonucleotide to (Figure 3C) or deletion of (Figure 5B) the *aRut* sequence. Moreover, the absence of RP2 products with the $[D^{aRut}D^{5del1}]R^{3u}O^1$ substrate (Figure 6D) supports ribose-specific secondary site activation (*5*, *9*, *32*, *33*, *41*) and Rho tracking on the upstream R^5 arm during RP2. In contrast, the unanticipated, yet dominant, RP1 tolerates the lack of a single-stranded *aRut* site within the forked substrate (Figures 3C and 5B) or the absence of 2′-OH groups in the upstream substrate's arm (Figure 6D). This suggests that, for RP1, Rho can make alternative compensatory primary contacts with the substrate and does not track on R^5 (see also below). With forked substrates devoid of *aRut* sequence, RP1 absolutely requires single-stranded RNA residues in the upstream substrate's arm (Figure 6B and data not shown) as well as glutamate ions in the mixture (Figure 5B). With forked substrates containing an *aRut* site, RNA residues in the upstream substrate's arm still potentiate RP1, but the effect is no longer dependent on the presence of glutamate ions (compare AcK graphs in panels C and D of Figure 6). Finally, in the absence of ribose moieties in the upstream substrate's arm, the presence of an *aRut* site is mandatory for RP1 to occur (Figure 6B,D and data not shown). Altogether, these data propound that RP1 stems from a larger set (and more kinds) of productive interactions with the substrate than RP2. These interactions include canonical primary contacts of Rho with *aRut* pyrimidine moieties (*3*, *4*, *10*) as well as unanticipated contacts between Rho and 2′-hydroxyl residues of the upstream substrate's arm (hereafter named noncanonical RP1 interactions) that are distinct

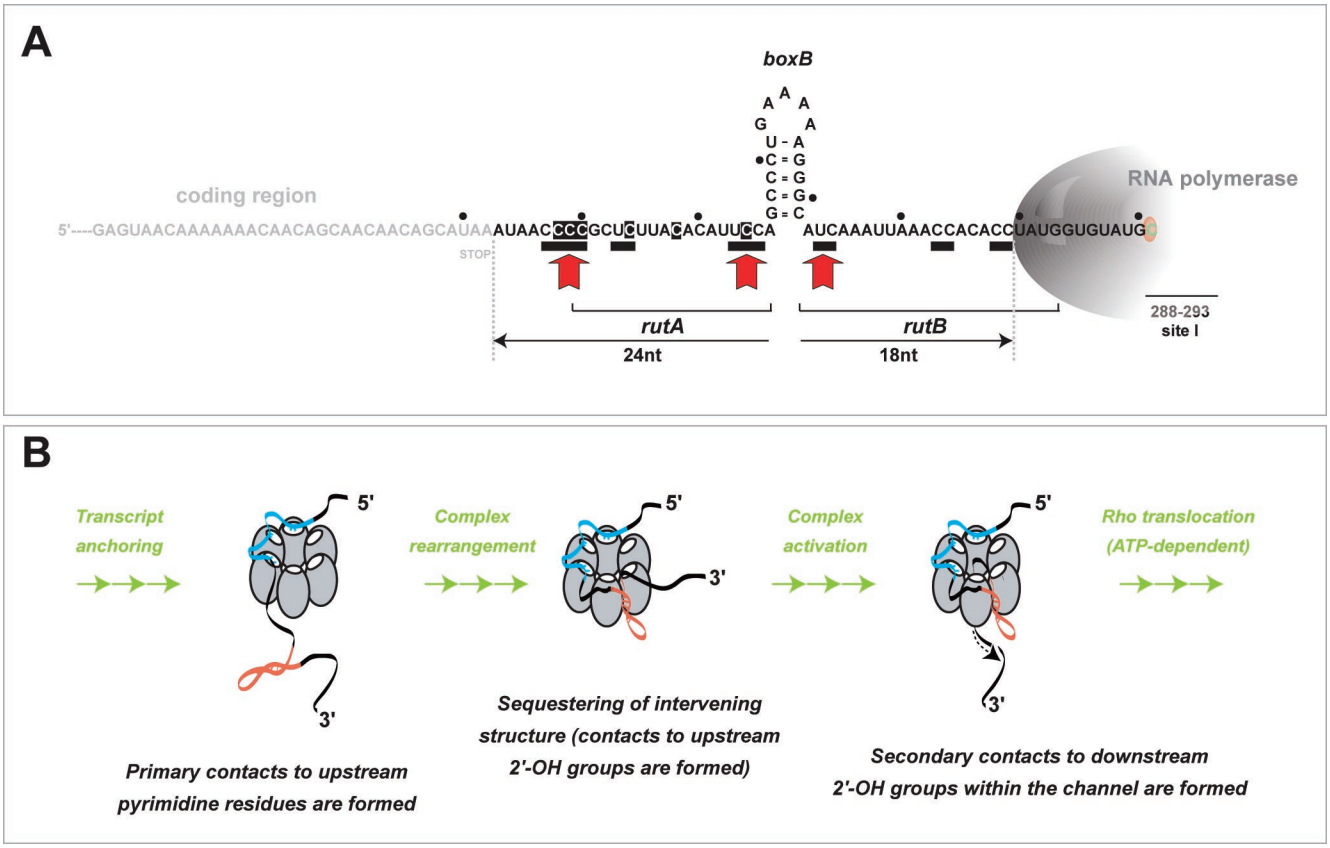

FIGURE 7: Interaction between a Rho hexamer and the nascent RNA transcript. (A) Schematic of the λtR1 termination system for the first cluster of transcript release sites (*13*, *45*, *47*, *48*). The upstream λcro coding sequence is colored gray; essential C residues in the *rutA* subsite (*46*) are highlighted with a black background, and 5′-YC dimers are underlined. The 3′-proximal transcript residue is colored green within the polymerase active site (orange). The red arrows denote 5′-YC dimers whose spacing (>30 Å) may allow concerted binding to a Rho primary binding site. Note, however, that additional interactions with isolated C residues (*10*) may also contribute to the primary binding of Rho to λtR1. (B) Schematic of the model of Brownian exploration of the Rho−substrate conformation for RP1. The Rho primary binding site is made of six monomer binding clefts (white ovals) that each can accommodate a 5′-YC dimer provided that the dimers are single-stranded and appropriately spaced (*4*, *8*). Following initial anchoring of Rho to a minimal single-stranded C-rich region of the transcript (blue), thermally driven fluctuations of the complex, including transient openings of the Rho ring (*8*, *11*), trigger the formation of additional tertiary interactions. We speculate that during this process the capture of a downstream RNA secondary structure through noncanonical interactions with Rho facilitates the transfer of downstream RNA into the central channel of the enzyme. Note, however, that stabilization of the primary Rho−transcript interaction may also involve the formation of supplementary sequence-specific contacts (*4*, *10*) of RNA with empty Rho subsites (not represented).

from the documented ribose-specific secondary site interactions that trigger Rho's ATPase (*5*, *8*, *32*, *33*). Although RP1 also benefits from the presence of the physiologically relevant glutamate ions (Figures 4A and 5B), the molecular origin of this effect remains obscure. It is possible that preferential exclusion of the glutamate ions from the protein−NA interface (*42*, *43*) favors the noncanonical RP1 interactions [note that ionic strength effects also suggest that the RP1 has a greater ionic content than RP2 (Figure 4D,E)]. Finally, the Y-shaped NA junction mandatory for RP1 (Figure 6A) may also provide an additional entropic advantage by reducing the conformational sampling of Rho−NA contacts. Alternatively, direct interactions between the double-stranded junction and Rho may provide further stabilization, a proposal that is, however, weakened (but not ruled out) by the absence of critical ribose moieties in one half of the junction helix (Figure 6B).

As stated above, the fact that RP1 can occur in the absence of RNA residues in the substrate's upstream arm (Figure 6D) argues against Rho skipping the intervening forked motif during translocation. Indeed, translocation of Rho along the upstream arm is ruled out if one assumes that RNA tracking is always mediated by contacts between 2′-OH and the Rho secondary binding site within the hexamer central channel (*5*, *8*, *32*, *33*). We thus favor a mechanism whereby Rho accommodates a native conformation of the forked motif within a composite primary interaction site. Rho translocation would then be restricted to single-stranded RNA downstream from the junction motif [provided that this single-stranded RNA is sufficiently long, i.e., ≥40 Å long, to be first accommodated in the central Rho channel (*9*), a proposal consistent with our observations; see Figure 3A]. In this case, RP1 binding may be preferred simply because it is an expanded version of the RP2 primary binding mode. Notably, RP1 binding would include contacts between Rho and 2′-OH groups of the upstream substrate's arm that are distinct from the documented Rho−RNA interactions (see the preceding paragraph). Although these noncanonical RP1 interactions do not seem to provide significant ground-state binding energy (see results and Table 1), they may stabilize and/or facilitate the transition to productive reaction intermediate(s). Accommodation of a secondary RNA structure within a composite Rho primary binding site is reminiscent of interaction of Rho with the natural λtR1 terminator (*12*−

14, *44*−*46*), though it is unknown in this case whether the intervening motif (boxB) remains native during the whole reaction pathway. Interestingly, the architecture and position of the λtR1 *Rut* site between the upstream coding region, coated by ribosomes, and the RNA 3′-ends defined by the first cluster of termination sites (*12*−*14*, *44*−*48*) preclude canonical primary binding of the transcript (i.e., 5′-YC-directed) to the six Rho primary subsites (Figure 7A). Additional facilitating interactions, such as the noncanonical contacts of RP1 with upstream 2′-OH groups, may thus also be relevant for the λtR1 terminator. These features could aid in the explanation of the glutamate potentiation of transcription termination at λtR1 (*49*). On the other hand, there are also noticeable differences between the λtR1 terminator and our composite RP1-promoting substrates. For instance, the λtR1 terminator is a compact system with a small hairpin structure right in the middle of the single-stranded C-rich sequence (Figure 7A; *12*, *13*, *44*). In contrast, single-stranded C residues within our composite substrates are scarce in the vicinity of the RNA junction (Figures 1B and 5A). Most primary interactions of Rho with this region should therefore be "noncanonical" (and include the unanticipated contacts between Rho and substrate's 2′-OH groups right in front of the forked motif). When present, the single-stranded C-rich *aRut* site is located far upstream from the RNA junction [there is an ∼80 nt spacer in the $R^5R^3O^n$ substrates (Figure 1B)], yet it can contribute significantly to RP1 (compare Figures 2A and 3C and Figures 4B and 6C). This suggests that RNA motifs that are different in nature (a single-stranded C-rich sequence and a forked structure), that possess distinct binding potentials (see results and Table 1), and that are distant from one another can still form a composite and advantageous primary binding site. From this perspective, however, one may wonder whether Rho binds the distant motifs simultaneously or sequentially. Equilibrium binding measurements, though they do not reflect the true potential for productive enzyme−NA interaction (*18*, *34*−*36*), demonstrated a preference of Rho for single-stranded C-rich NA strands (Table 1; *6*, *18*, *30*, *50*). Thus, the classical view that single-stranded C-rich RNA segments serve as primary anchor points (*1*, *2*) also probably holds true in the present case. Once bound to a C-rich sequence, Rho may then scan downstream regions for RNA motifs capable of further stabilizing and/or activating the enzyme−substrate complex (Figure 7B). Brownian exploration of the Rho−substrate conformation and accommodation of downstream RNA motifs into a composite Rho primary binding site may thus provide a low-cost alternative to ATPase-driven translocation of the enzyme along the corresponding transcript region. This plasticity of RNA recognition by Rho is consistent with relaxed compositional rules for Rho-dependent terminators (*1*, *2*) and could explain, at least in part, the spread of Rho-dependent termination sites (*1*), especially if Rho action is always rate-limited by the same postbinding step (*22*). We observe that such sequential sampling and accommodation of primary binding components (Figure 7B) is also in line with the looping out model that was put forth by von Hippel and co-workers to explain the modulation of the *trpt*′ termination zone as a function of the amount of secondary structures within the nascent transcript (*17*). From this perspective, it is worth noting that Rho may not sample each individual nucleotide during its progression along the RNA track and that this behavior may be distinct from those of other RNA translocases. However, we also acknowledge that various molecular details of the relaxed RP1 binding mode remain elusive and that features of the models presented in Figure 7C will require further investigation. In doing so, minimal forked substrates such as the ones used in this work (Figures 5 and 6) may again prove themselves advantageous. Indeed, by constraining the initial Rho−substrate conformation (thereby reducing the number of starting species) and by restricting Rho translocation to the downstream R^3 arm, the forked junction should facilitate the isolation and study of specific substrate features, Rho−NA interactions, and steps of the enzyme cycle.

ACKNOWLEDGMENT

We gratefully acknowledge J. P. Richardson and P. H. von Hippel for the gift of materials.

REFERENCES

1. Richardson, J. P. (2002) Rho-dependent termination and ATPases in transcript termination, *Biochim. Biophys. Acta 1577*, 251−260.
2. Ciampi, M. S. (2006) Rho-dependent terminators and transcription termination, *Microbiology 152*, 2515−2528.
3. Richardson, L. V., and Richardson, J. P. (1992) Cytosine nucleoside inhibition of the ATPase of *Escherichia coli* termination factor rho: Evidence for a base specific interaction between rho and RNA, *Nucleic Acids Res. 20*, 5383−5387.
4. Bogden, C. E., Fass, D., Bergman, N., Nichols, M. D., and Berger, J. M. (1999) The structural basis for terminator recognition by the Rho transcription termination factor, *Mol. Cell 3*, 487−493.
5. Richardson, J. P. (1982) Activation of rho protein ATPase requires simultaneous interaction at two kinds of nucleic acid-binding sites, *J. Biol. Chem. 257*, 5760−5766.
6. McSwiggen, J. A., Bear, D. G., and von Hippel, P. H. (1988) Interactions of *Escherichia coli* transcription termination factor rho with RNA. I. Binding stoichiometries and free energies, *J. Mol. Biol. 199*, 609−622.
7. Briercheck, D. M., Allison, T. J., Richardson, J. P., Ellena, J. F., Wood, T. C., and Rule, G. S. (1996) ^{1}H, ^{15}N and ^{13}C resonance assignments and secondary structure determination of the RNA-binding domain of *E. coli* rho protein, *J. Biomol. NMR 8*, 429−444.
8. Skordalakes, E., and Berger, J. M. (2003) Structure of the rho transcription terminator. Mechanism of mRNA recognition and helicase loading, *Cell 114*, 135−146.
9. Skordalakes, E., and Berger, J. M. (2006) Structural Insights into RNA-Dependent Ring Closure and ATPase Activation by the Rho Termination Factor, *Cell 127*, 553−564.
10. Hitchens, T. K., Zhan, Y., Richardson, L. V., Richardson, J. P., and Rule, G. S. (2006) Sequence-specific Interactions in the RNA-binding Domain of *Escherichia coli* Transcription Termination Factor Rho, *J. Biol. Chem. 281*, 33697−33703.
11. Kim, D. E., and Patel, S. S. (2001) The kinetic pathway of RNA binding to the *Escherichia coli* transcription termination factor Rho, *J. Biol. Chem. 276*, 13902−13910.
12. Chen, C. Y., and Richardson, J. P. (1987) Sequence elements essential for rho-dependent transcription termination at λtR1, *J. Biol. Chem. 262*, 11292−11299.
13. Faus, I., and Richardson, J. P. (1990) Structural and functional properties of the segments of λcro mRNA that interact with transcription termination factor Rho, *J. Mol. Biol. 212*, 53−66.
14. Vieu, E., and Rahmouni, A. R. (2004) Dual role of boxB RNA motif in the mechanisms of termination/antitermination at the λtR1 terminator revealed in vivo, *J. Mol. Biol. 339*, 1077−1087.
15. Steinmetz, E. J., Brennan, C. A., and Platt, T. (1990) A short intervening structure can block rho factor helicase action at a distance, *J. Biol. Chem. 265*, 18408−18413.
16. Zhu, A. Q., and von Hippel, P. H. (1998) Rho-dependent termination within the trp t′ terminator. I. Effects of rho loading and template sequence, *Biochemistry 37*, 11202−11214.
17. Zhu, A. Q., and von Hippel, P. H. (1998) Rho-dependent termination within the trp t′ terminator. II. Effects of kinetic competition and rho processivity, *Biochemistry 37*, 11215−11222.

18. Walmacq, C., Rahmouni, A. R., and Boudvillain, M. (2004) Influence of substrate composition on the helicase activity of transcription termination factor Rho: Reduced processivity of Rho hexamers during unwinding of RNA-DNA hybrid regions, *J. Mol. Biol. 342*, 403−420.
19. Gai, D., Zhao, R., Li, D., Finkielstein, C. V., and Chen, X. S. (2004) Mechanisms of conformational change for a replicative hexameric helicase of SV40 large tumor antigen, *Cell 119*, 47−60.
20. Yu, X., Horiguchi, T., Shigesada, K., and Egelman, E. H. (2000) Three-dimensional reconstruction of transcription termination factor rho: Orientation of the N-terminal domain and visualization of an RNA-binding site, *J. Mol. Biol. 299*, 1279−1287.
21. Guerin, M., Robichon, N., Geiselmann, J., and Rahmouni, A. R. (1998) A simple polypyrimidine repeat acts as an artificial Rho-dependent terminator in vivo and in vitro, *Nucleic Acids Res. 26*, 4895−4900.
22. Walmacq, C., Rahmouni, A. R., and Boudvillain, M. (2006) Testing the steric exclusion model for hexameric helicases: Substrate features that alter RNA-DNA unwinding by the transcription termination factor Rho, *Biochemistry 45*, 5885−5895.
23. Schwartz, A., Rahmouni, A. R., and Boudvillain, M. (2003) The functional anatomy of an intrinsic transcription terminator, *EMBO J. 22*, 3385−3394.
24. Persson, T., Willkomm, D. K., and Hartmann, R. K. (2005) T4 RNA ligase, in *Handbook of RNA Biochemistry* (Hartmann, R. K., Bindereif, A., Schön, A., and Westhof, E., Eds.) pp 53−74, Wiley-VCH, Weinheim, Germany.
25. Brennan, C. A., Steinmetz, E. J., Spear, P., and Platt, T. (1990) Specificity and efficiency of rho-factor helicase activity depends on magnesium concentration and energy coupling to NTP hydrolysis, *J. Biol. Chem. 265*, 5440−5447.
26. Sugimoto, N., Nakano, S., Katoh, A., Nakamura, H., Ohmichi, T., Yoneyama, M., and Sasaki, M. (1995) Thermodynamic Parameters to Predict the Stability of RNA/DNA Hybrid Duplexes, *Biochemistry 34*, 11211−11216.
27. Xia, T., SantaLucia, J., Jr., Burkard, M. E., Kierzek, R., Schroeder, S. J., Jiao, X., Cox, C., and Turner, D. H. (1998) Thermodynamic parameters for an expanded nearest-neighbor model for formation of RNA duplexes with Watson-Crick base pairs, *Biochemistry 37*, 14719−14735.
28. Walstrom, K. M., Dozono, J. M., Robic, S., and von Hippel, P. H. (1997) Kinetics of the RNA-DNA helicase activity of *Escherichia coli* transcription termination factor rho. 1. Characterization and analysis of the reaction, *Biochemistry 36*, 7980−7992.
29. Brennan, C. A., Dombroski, A. J., and Platt, T. (1987) Transcription termination factor rho is an RNA-DNA helicase, *Cell 48*, 945−952.
30. Wang, Y., and von Hippel, P. H. (1993) *Escherichia coli* transcription termination factor rho. II. Binding of oligonucleotide cofactors, *J. Biol. Chem. 268*, 13947−13955.
31. Geiselmann, J., Yager, T., Gill, S., Calmettes, P., and von Hippel, P. (1992) Physical properties of the *Escherichia coli* transcription termination factor rho. 1. Association states and geometry of the rho hexamer, *Biochemistry 31*, 111−121.
32. Wei, R. R., and Richardson, J. P. (2001) Mutational changes of conserved residues in the Q-loop region of transcription factor Rho greatly reduce secondary site RNA-binding, *J. Mol. Biol. 314*, 1007−1015.
33. Wei, R. R., and Richardson, J. P. (2001) Identification of an RNA-binding site in the ATP binding domain of *Escherichia coli* Rho by H_2O_2/Fe-EDTA cleavage protection studies, *J. Biol. Chem. 276*, 28380−28387.
34. Pang, P. S., Jankowsky, E., Planet, P. J., and Pyle, A. M. (2002) The hepatitis C viral NS3 protein is a processive DNA helicase with cofactor enhanced RNA unwinding, *EMBO J. 21*, 1168−1176.
35. Wang, Y., and von Hippel, P. H. (1993) *Escherichia coli* transcription termination factor rho. I. ATPase activation by oligonucleotide cofactors, *J. Biol. Chem. 268*, 13940−13946.
36. Zalatan, F., and Platt, T. (1992) Effects of decreased cytosine content on rho interaction with the rho-dependent terminator trp t′ in *Escherichia coli*, *J. Biol. Chem. 267*, 19082−19088.
37. Jankowsky, E., Fairman, M. E., and Yang, Q. (2005) RNA helicases: Versatile ATP-driven nanomotors, *J. Nanosci. Nanotechnol. 5*, 1983−1989.
38. Eoff, R. L., and Raney, K. D. (2005) Helicase-catalysed translocation and strand separation, *Biochem. Soc. Trans. 33*, 1474−1478.
39. Aguilera, A. (2005) Cotranscriptional mRNP assembly: From the DNA to the nuclear pore, *Curr. Opin. Cell Biol. 17*, 242−250.
40. Pan, T., and Sosnick, T. (2006) RNA Folding During Transcription, *Annu. Rev. Biophys. Biomol. Struct.* (doi, 10.1146/annurev.biophys.35.040405.102053).
41. Chen, X., and Stitt, B. L. (2004) The binding of C10 oligomers to *Escherichia coli* transcription termination factor Rho, *J. Biol. Chem. 279*, 16301−16310.
42. Courtenay, E. S., Capp, M. W., Anderson, C. F., and Record, M. T., Jr. (2000) Vapor pressure osmometry studies of osmolyte-protein interactions: Implications for the action of osmoprotectants in vivo and for the interpretation of "osmotic stress" experiments in vitro, *Biochemistry 39*, 4455−4471.
43. Ha, J. H., Capp, M. W., Hohenwalter, M. D., Baskerville, M., and Record, M. T., Jr. (1992) Thermodynamic stoichiometries of participation of water, cations and anions in specific and non-specific binding of lac repressor to DNA. Possible thermodynamic origins of the "glutamate effect" on protein-DNA interactions, *J. Mol. Biol. 228*, 252−264.
44. Chen, C. Y., Galluppi, G. R., and Richardson, J. P. (1986) Transcription termination at λtR1 is mediated by interaction of rho with specific single-stranded domains near the 3′ end of cro mRNA, *Cell 46*, 1023−1028.
45. Graham, J. E., and Richardson, J. P. (1998) rut Sites in the nascent transcript mediate Rho-dependent transcription termination in vivo, *J. Biol. Chem. 273*, 20764−20769.
46. Graham, J. E. (2004) Sequence-specific Rho-RNA interactions in transcription termination, *Nucleic Acids Res. 32*, 3093−3100.
47. Morgan, W. D., Bear, D. G., and von Hippel, P. H. (1983) Rho-dependent termination of transcription. I. Identification and characterization of termination sites for transcription from the bacteriophage λPR promoter, *J. Biol. Chem. 258*, 9553−9564.
48. Lau, L. F., Roberts, J. W., and Wu, R. (1982) Transcription terminates at λtR1 in three clusters, *Proc. Natl. Acad. Sci. U.S.A. 79*, 6171−6175.
49. Zou, L. L., and Richardson, J. P. (1991) Enhancement of transcription termination factor rho activity with potassium glutamate, *J. Biol. Chem. 266*, 10201−10209.
50. Faus, I., and Richardson, J. P. (1989) Thermodynamic and enzymological characterization of the interaction between transcription termination factor rho and λcro mRNA, *Biochemistry 28*, 3510−3517.

BI700493M